

Anisotropic thermal expansion and uniaxial pressure dependence of superconducting and magnetic transitions in $\text{ErNi}_2\text{B}_2\text{C}$.

S.L. Bud'ko^a, G.M. Schmiedeshoff^b, P.C. Canfield^a

^a*Ames Laboratory US DOE and Department of Physics and Astronomy, Iowa State University, Ames, IA 50011, USA*

^b*Department of Physics, Occidental College, Los Angeles, CA 90041, USA*

Abstract

We present anisotropic thermal expansion measurements on single crystalline $\text{ErNi}_2\text{B}_2\text{C}$. All three, superconducting, antiferromagnetic and weak ferromagnetic phase transitions are unambiguously distinguished in the data. Anisotropic uniaxial pressure dependencies of the transitions are estimated based on the Ehrenfest relation, leading to a conclusion, in particular, that weak ferromagnetic state will be suppressed by small, order of several kbar, hydrostatic pressure.

Key words: A. magnetically ordered materials, A. superconductors, D. thermal expansion

PACS: 65.40.De, 74.70.Dd, 75.30.Kz, 75.40.Cx, 75.80.+q

Quaternary borocarbides, in particular the members of the $R\text{Ni}_2\text{B}_2\text{C}$ ($R = \text{Gd-Lu, Y}$) series of compounds, exhibit a plethora of complex phenomena: co-existence of local moment magnetism and superconductivity, non-locality and flux line lattice transitions, heavy fermion physics and intricate metamagnetism [1,2,3,4]. $\text{ErNi}_2\text{B}_2\text{C}$ superconducts below ~ 10 K [5,6], below $T_N \approx 6$ K superconductivity coexists with an incommensurate antiferromagnetic state with the ordering wave vector $\mathbf{q} \approx 0.55 \mathbf{a}^*$ [8,9,7], and then, on further cooling, a weak ferromagnetic component develops below $T_{WFM} \approx 2.3$ K [10,11,12].

Despite a large number of publications on physical properties of $\text{ErNi}_2\text{B}_2\text{C}$, few of them address temperature dependent structural changes in the material. The evolution of the lattice parameters between 360 K and 90 K, as measured by single crystal X-ray diffraction, was reported in Ref. [13]. A magnetoelastic tetragonal-to-orthorhombic structural distortion was observed [14] below T_N by synchrotron X-ray scattering. A λ -type anomaly in thermal expansion at

T_N was reported in STM measurements [15]. And finally, a low temperature $H - T$ phase diagram was probed [16] using thermal expansion (in an applied field) and magnetostriction measurements.

In this publication we report high resolution, anisotropic (c -axis and a -axis) thermal expansion (TE) and longitudinal, low temperature, magnetostriction (MS) measurements for $H \parallel a$ on single crystalline $\text{ErNi}_2\text{B}_2\text{C}$. These measurements were performed with the intent to study the anomalies in TE associated with all three salient transition temperatures (to the best of our knowledge, for two of them, T_c and T_{WFM} , no TE anomalies were reported so far) and to evaluate the uniaxial pressure derivatives of the three transition temperatures using the the thermodynamic Ehrenfest relation.

Plate-like single crystals of $\text{ErNi}_2\text{B}_2\text{C}$ with the c -axis perpendicular to the plates were grown by a Ni_2B high temperature flux method (see Refs. [1,7,17,18] for more details). For the TE/MS measurements the $\text{ErNi}_2\text{B}_2\text{C}$ crystal was shaped into a nearly rectangular bar, with two pairs of parallel surfaces, so that the measurements were performed along [100] ($L = 2.23$ mm) and [001] ($L = 1.42$ mm) directions. After shaping, the sample was annealed in dynamic vacuum ($10^{-5} - 10^{-6}$ Torr) at 950°C for ~ 100 hours [19]. Thermal expansion and magnetostriction were measured using a capacitive dilatometer constructed of OFHC copper; a detailed description of the dilatometer will appear elsewhere [20]. The dilatometer was mounted in a Quantum Design PPMS-14 instrument and was operated over a temperature range of 1.8 to 305 K and in magnetic fields up to 140 kOe. The same set-up was used in our recent work on $\text{YNi}_2\text{B}_2\text{C}$ [21]. Heat capacity was measured using a heat capacity option with ^3He insert of a PPMS instrument. DC magnetization was measured using a Quantum Design MPMS-7 SQUID magnetometer.

The temperature-dependent linear (α_a , α_c) and volume ($\beta = 2\alpha_a + \alpha_c$) thermal expansion coefficients are shown in Fig. 1. Data for $T \geq 100$ K are in a good agreement with the previously reported results [13] (shown as open symbols in Fig. 1(a)). Clear anomalies are detected at T_N and T_{WFM} (Fig. 1(b)). The size of the (inverse) λ -like anomaly in α_c at T_N is similar to the value reported in Ref. [15]. On cooling down from just above T_N the α_a initially increases and then goes into sharp, deep minimum. Such behavior (as opposed to some sort of λ -like anomaly) may be associated with possible formation of the antiferromagnetic domains (twins) in the crystal in zero or small fields [22,23] due to orthorhombic structural distortion below T_N [14]. The complexity of in-plane thermal expansion of $\text{ErNi}_2\text{B}_2\text{C}$ near T_N is illustrated in Fig. 2: whereas for $H \parallel c$ an application of 2 kOe field does not change the temperature-dependent dilation (and the TE coefficient), field applied along a -axis changes the longitudinal dilation dramatically. These results are consistent with higher fields study in Ref. [16]. Jumps in α_a and α_c associated with the superconducting transition are small but unequivocal in the data (Fig. 1(c)). The values of $\Delta\alpha_a$

and $\Delta\alpha_c$ at T_c are of the same order of magnitude as in $\text{YNi}_2\text{B}_2\text{C}$ [21], but of the opposite signs. The temperatures associated with the anomalies in the TE coefficients are consistent with the phase transitions observed in heat capacity (Fig. 3).

Using results from the heat capacity (Fig. 3) and thermal expansion coefficients (Fig. 1) measurements, the uniaxial pressure derivatives of the phase transition temperatures, T_c , T_N and T_{WFM} , can be calculated using the thermodynamic Ehrenfest relation for the second order phase transitions:

$$\frac{dT_{crit}}{dp_i} = V_{mol} \cdot \Delta\alpha_i(T_{crit}) \cdot \left[\frac{\Delta C_p(T_{crit})}{T_{crit}} \right]^{-1}$$

where V_{mol} is a molar volume of the material (for $\text{ErNi}_2\text{B}_2\text{C}$, $V_{mol} = 39.2 \text{ cm}^3$) and $\Delta\alpha_i(T_{crit})$ and $\Delta C_p(T_{crit})$ are the jumps in the i -th thermal expansion coefficient and specific heat at T_{crit} . Estimates of the uniaxial pressure derivatives for $\text{ErNi}_2\text{B}_2\text{C}$ based on the aforementioned measurements are summarized in Table 1. Due to complex behavior of α_a at T_N , we were not able to estimate dT_N/dp_a and dT_N/dP^* . The error bars for the uniaxial pressure derivatives listed in the Table 1 are rather large, possibly up to 30–50 % due to signal to noise ratio in the temperature-dependent TE coefficient data and possible ambiguity in ΔT_{crit} determination at T_c and T_{WFM} .

In the table $dT_{crit}/dP^* = 2 \cdot dT_{crit}/dp_{ab} + dT_{crit}/dp_c$. The dT_{crit}/dP^* defined in such way lacks the contribution from the off-diagonal dT_{crit}/dp_{ij} , $i \neq j$ terms that play a role in the experimentally measured dT_c/dP under hydrostatic pressure. Since the off-diagonal terms are usually significantly smaller than the diagonal ones, we can still compare the last column of the Table 1 with the experimentally measured hydrostatic pressure derivatives. The hydrostatic pressure measurements on $\text{ErNi}_2\text{B}_2\text{C}$ are rather sparse: there were two reports on initial ($P \rightarrow 0$) dT_c/dP [24,25] with the values of different signs, $-0.82 \times 10^{-2} \text{ K/kbar}$ and $+1.68 \times 10^{-2}$ respectively, T_N was reported to increase under pressure [26] and no data for T_{WFM} under pressure are available so far. For T_c our estimates, within the restrictions mentioned above, are qualitatively consistent with the small and negative dT_c/dP reported in Ref. [24]. Our results predict high sensitivity of both T_N and T_{WFM} to uniaxial pressure. Within the above analysis, we can expect that the weak ferromagnetic state is very fragile and hydrostatic pressure as moderate as 1 kbar will drive T_{WFM} to zero. It will require heat capacity measurements under pressure to verify this prediction. It is curious that whereas T_c is almost pressure independent and T_N and T_{WFM} appear to be very pressure sensitive, another perturbation to the material, Co doping to the Ni site, yields the opposite effect [27]: already 6% of Co in $\text{Er}(\text{Ni}_{1-x}\text{Co}_x)_2\text{B}_2\text{C}$ brings T_c down to below 2 K, while 8% of Co causes decrease of T_N only by ~ 0.5 K and has almost no effect on T_{WFM} . Comparison of these two perturbations suggests that steric effects are well

separated from band-filling effects in $\text{ErNi}_2\text{B}_2\text{C}$.

Longitudinal magnetostriction of $\text{ErNi}_2\text{B}_2\text{C}$ for $L \parallel H \parallel a$ is shown in Fig. 4. In the overlapping temperature range our data are consistent with the results of Ref. [16]. At base temperature (1.8 K) features associated with four metamagnetic transitions can be distinguished in the derivative of magnetostriction with respect to magnetic field (Fig. 5), consistent with (within errors of orientation) with the magnetization data. The base temperature magnetostriction data suggest that, in agreement with earlier magnetization studies [10,28,29] the $H - T$ phase diagram for $\text{ErNi}_2\text{B}_2\text{C}$ is richer and more complex than suggested in Ref. [16].

In summary, thermal expansion measurements combined with temperature-dependent specific heat data, allow us to estimate uniaxial pressure dependencies of three phase transitions in $\text{ErNi}_2\text{B}_2\text{C}$, superconducting, antiferromagnetic and weak ferromagnetic. Our data are roughly consistent with the results of hydrostatic pressure effect on superconducting transition temperature. Both, Néel and weak ferromagnetic ordering temperature are envisaged to be very sensitive to stress/pressure. Additionally, magnetostriction is shown to be a useful probe for rich and complex $H - T$ phase diagram in this material.

Acknowledgements

Ames Laboratory is operated for the U. S. Department of Energy by Iowa State University under Contract No. W-7405-Eng.-82. This work was supported by the director for Energy Research, Office of Basic Energy Sciences. One of us (GMS) is supported by the National Science Foundation under DMR-0305397. We thank V. Pelevin for his useful suggestion regarding comparative mensuration.

References

- [1] P. C. Canfield, P. L. Gammel, D. J. Bishop, Phys. Today **51**(10), 47 (1998).
- [2] K.-H. Müller, V. N. Narozhnyi, Rep. Progr. Phys. **64**, 943 (2001).
- [3] K.-H. Müller, G. Fuchs, S.-L. Drechsler, V. N. Narozhnyi in: K. H. J. Buschow (Ed.) *Handbook of Magnetic Materials* vol. 14 (Amsterdam: North-Holland) p. 199, 2002.
- [4] S. L. Bud'ko, P. C. Canfield, C. R. Physique **7** 56 (2006).

- [5] R. J. Cava, H. Takagi, B. Batlogg, H. W. Zandbergen, J. J. Krajewski, W. F. Peck Jr., R. B. van Dover, R. J. Felder, T. Siegrist, K. Mizuhashi, J. O. Lee, H. Eisaki, S. Uchida, *Nature* **367**, 252 (1994).
- [6] H. Eisaki, H. Takagi, R. J. Cava, B. Batlogg, J. J. Krajewski, W. F. Peck Jr., K. Mizuhashi, J. O. Lee, S. Uchida, *Phys. Rev. B* **50**, 647 (1994).
- [7] B. K. Cho, P.C. Canfield, L. L. Miller, D. C. Johnston, W. P. Beyermann, A. Yatskar, *Phys. Rev. B* **52**, 3684 (1995).
- [8] J. Zarestky, C. Stassis, A.I. Goldman, P.C. Canfield, P. Dervenagias, B. K. Cho, D. C. Johnston, *Phys. Rev. B* **51**, 678 (1995).
- [9] S. K. Sinha, J. W. Lynn, T. E. Grigereit, Z. Hossain, L. C. Gupta, R. Nagarajan, C. Godart, *Phys. Rev. B* **51**, 684 (1995).
- [10] P.C. Canfield, S. L. Bud'ko, B. K. Cho, *Physica C* **262**, 249 (1996).
- [11] S.-M. Choi, J. W. Lynn, D. Lopez, P. L. Gammel, P.C. Canfield, S. L. Bud'ko, *Phys. Rev. Lett.* **87**, 107001 (2001).
- [12] H. Kawano-Furukawa, H. Takeshita, M. Ochiai, T. Nagata, H. Yoshizawa, H. Takeya, K. Kadowaki, *Phys. Rev. B* **65**, 180508 (2002).
- [13] U. Jaenicke-Roessler, P. Paufler, G. Zahn, S. Geupel, G. Behr, H. Bitterlich, J. Alloys Compd. **333**, 28 (2002).
- [14] C. Detlefs, A. H. M. Z. Islam, T. Gu, A.I. Goldman, C. Stassis, P.C. Canfield, J. P. Hill, T. Vogt, *Phys. Rev. B* **56**, 7843 (1997).
- [15] M. Crespo, H. Suderow, S. Vieira, S. Bud'ko, P. C. Canfield, *Physica B* **378-380**, 471 (2006).
- [16] M. Doerr, M. Rotter, M. El Massalami, S. Sinning, H. Takeya, M. Loewenhaupt, *J. Phys.: Cond. Mat.* **14**, 5609 (2002).
- [17] M. Xu, P. C. Canfield, J. E. Ostenson, D. K. Finnemore, B. K. Cho, Z. R. Wang, D. C. Johnston, *Physica C* **227** 321 (1994).
- [18] P. C. Canfield, I. R. Fisher, *J. Crystal Growth* **225** 155 (2001).
- [19] X. Y. Miao, S. L. Bud'ko, P. C. Canfield, *J. Alloys Compd.* **338** 13 (2002).
- [20] G. M. Schmiedeshoff, in preparation.
- [21] S. L. Bud'ko, G. M. Schmiedeshoff, G. Lapertot, P. C. Canfield, preprint [cond-mat/0606746](http://arxiv.org/abs/cond-mat/0606746) (2006).
- [22] L. Ya. Vinnikov, J. Anderegg, S. L. Bud'ko, P. C. Canfield, V. G. Kogan, *Phys. Rev. B* **71** 224513 (2005).
- [23] H. Bluhm, S. E. Sebastian, J. W. Guikema, I. R. Fisher, K. A. Moler, *Phys. Rev. B* **73** 014514 (2006).
- [24] H. Schmidt, H. F. Braun, *Physica C* **229** 315 (1994).

- [25] E. Alleno, J. J. Neumeier, J.D. Thompson, P. C. Canfield, B. K. Cho, *Physica C* **242** 1694 (1995).
- [26] N. Matsuda, H. Setoguchi, T. Kagayama, G. Oomi, B. K. Cho, P. C. Canfield, *Physica B* **281&282** 1001 (2000).
- [27] S. L. Bud'ko, P. C. Canfield, *Physica B* **280** 356 (2000).
- [28] P. C. Canfield, S. L. Bud'ko, *J. Alloys Compd.* **262-263** 169 (1997).
- [29] S. L. Bud'ko, P. C. Canfield, *Phys. Rev. B* **61** R14932 (2000).

Table 1

Changes in specific heat and thermal expansion coefficients at three ordering temperatures, T_{crit} , for superconducting (SC), antiferromagnetic (AFM) and weak ferromagnetic (WFM) phase transitions and estimates of their anisotropic pressure derivatives.

transition	T_{crit} (K)	ΔC_p (J/mol K)	$\Delta\alpha_a$ (10^{-6} K $^{-1}$)	$\Delta\alpha_c$ (10^{-6} K $^{-1}$)	dT_{crit}/dp_a (K/kbar)	dT_{crit}/dp_c (K/kbar)	dT_{crit}/dP^* (K/kbar)
SC	10.1	0.24	0.01	-0.08	$1.6 \cdot 10^{-2}$	$-13 \cdot 10^{-2}$	$-9.8 \cdot 10^{-2}$
AFM	6.1	23.3		-117		-1.2	
WFM	2.3	0.6	-9.0	-1.4	-1.4	-0.2	-3

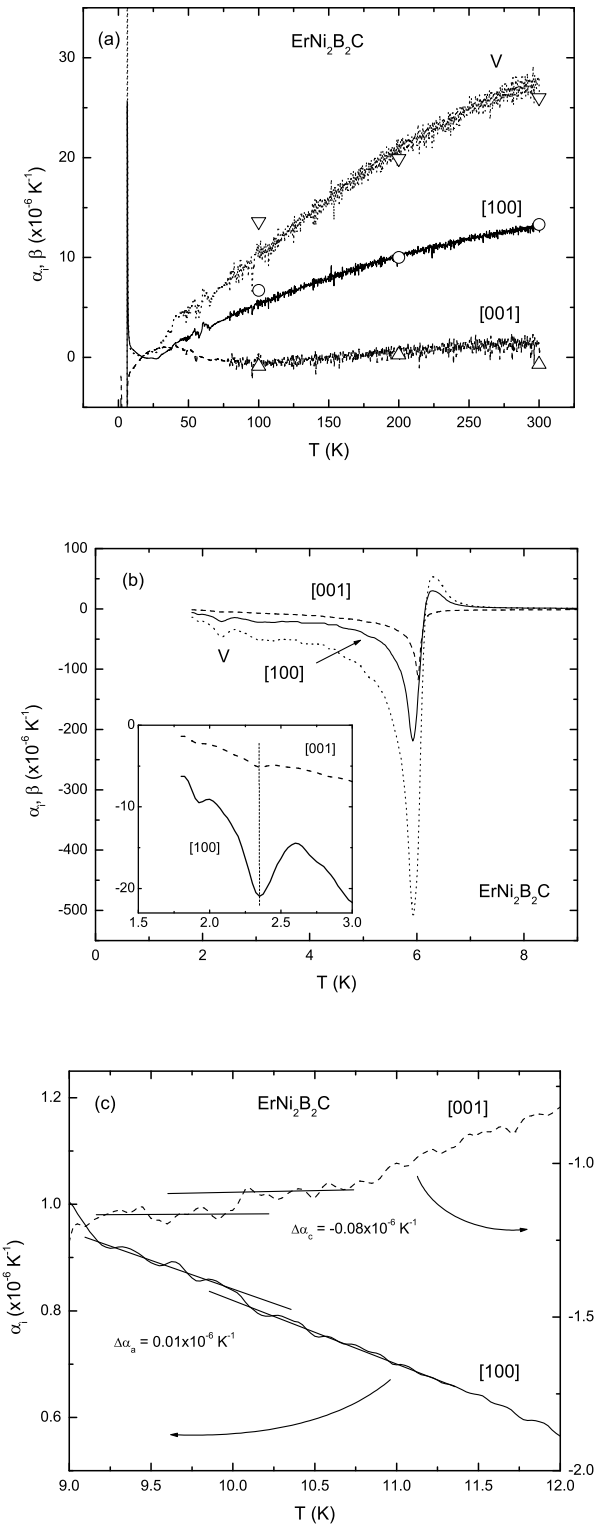


Fig. 1. The temperature-dependent linear and volume thermal expansion coefficients of $\text{ErNi}_2\text{B}_2\text{C}$. Open symbols in (a) are data from Ref. [13]. (b) low temperature thermal expansion, inset - enlarged view near the transition to weak ferromagnetic phase, T_{WFM} is marked with a vertical line. (c) linear TE coefficients near superconducting transition.

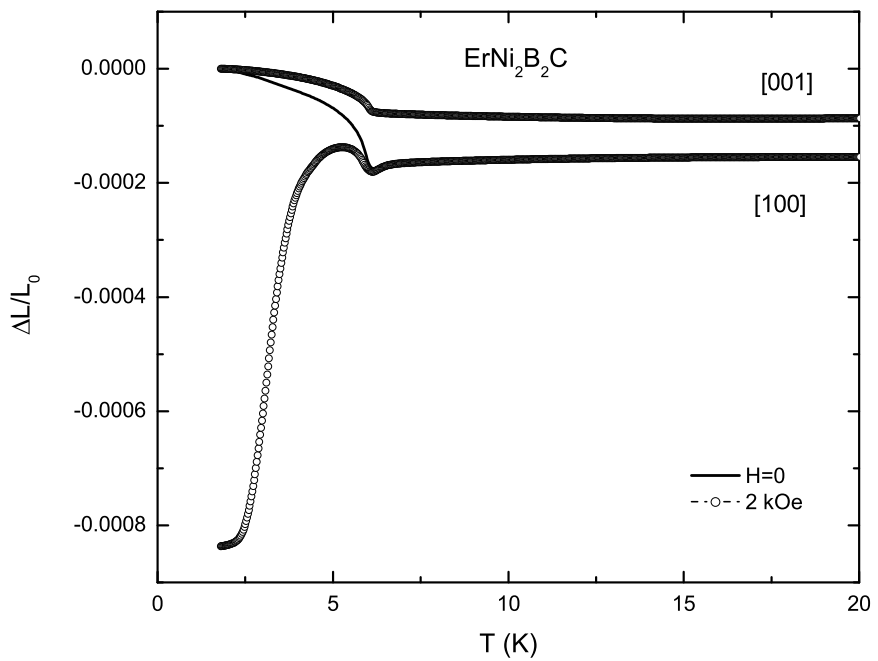


Fig. 2. Low temperature longitudinal dilation of $\text{ErNi}_2\text{B}_2\text{C}$ in zero and 2 kOe applied field plotted relatively to the $T = 1.8$ K, $H = 0$ (L_0) value. For [001] the $H = 0$ and $H = 2$ kOe lines are indistinguishable on the scale of the graph.

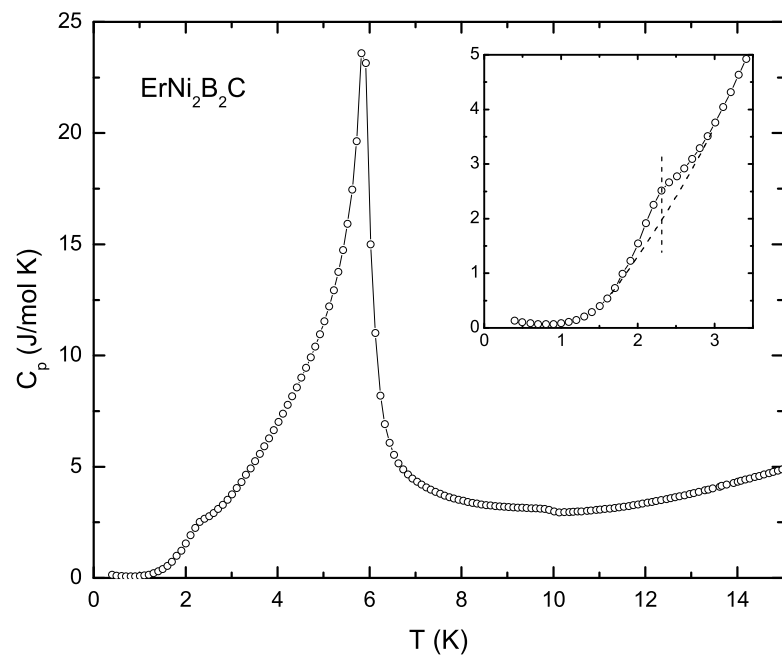


Fig. 3. Temperature-dependent heat capacity of $\text{ErNi}_2\text{B}_2\text{C}$. Inset: enlarged region near T_{WFM} with a sketch of an estimate of ΔC_p at T_{WFM} .

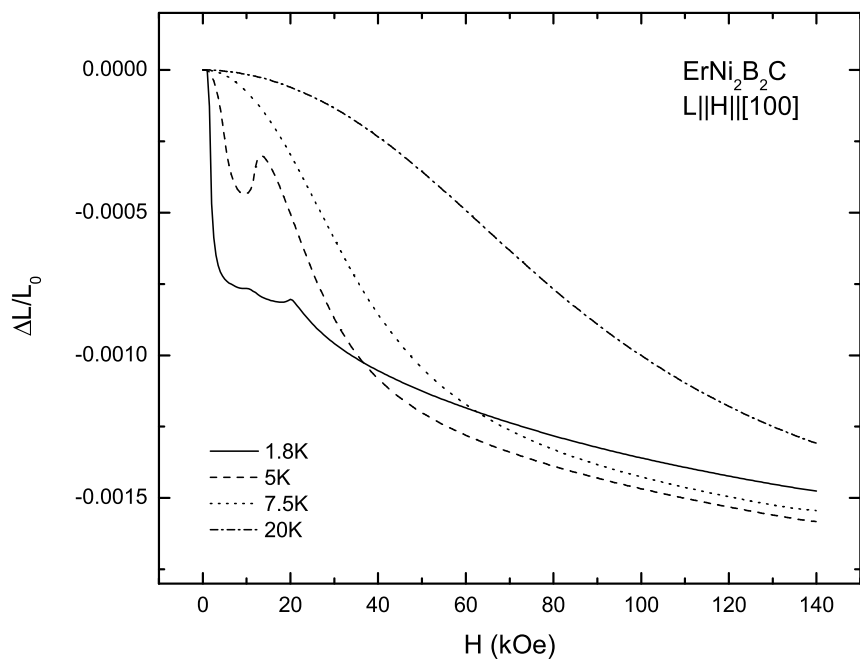


Fig. 4. Longitudinal magnetostriction of $\text{ErNi}_2\text{B}_2\text{C}$ measured for $H \parallel a$.

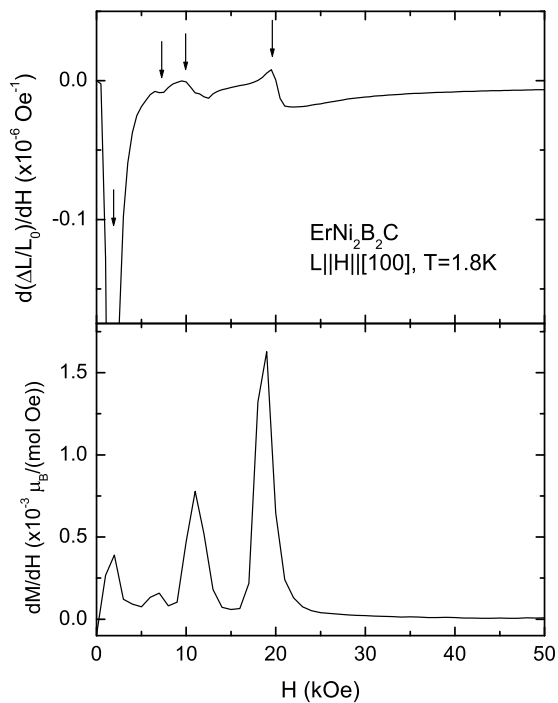


Fig. 5. Upper panel - derivative of magnetostriction with respect to magnetic field for $H \leq 50$ kOe. Dip at ~ 1.9 kOe reaches -4.75×10^{-7} Oe $^{-1}$. Arrows mark features associated with the metamagnetic transitions. Lower panel - derivative of magnetization with respect to magnetic field for the same orientation.